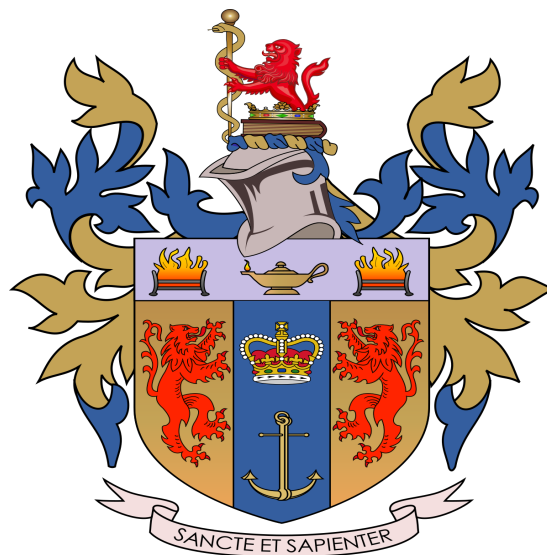

Multiscale Modelling of Indium Phosphide Quantum Dots

WRITTEN BY FRAN PANTELI

SUPERVISED BY DR ALEJANDRO
SANTANA-BONILLA & PROFESSOR CHRIS
LORENZ

September 2022

King's College London Department of Natural &
Mathematical Sciences



Contents

1	Introduction	3
1.1	An Introduction to Indium Phosphide Quantum Dots	3
1.2	The Structure & Properties of Crystalline InP	4
1.2.1	Structure & Bonding Within InP	4
1.2.2	Electronic Structure Properties of InP	4
1.3	InP QDs	6
1.3.1	The Structure of InP QDs	6
1.3.2	Numerical Techniques For Simulating InP QDs	8
1.3.3	Challenges When Simulating InP QDs	9
2	Results & Analysis	10
3	Conclusion	13
4	Supplementary Information	16
4.0.1	Theory for Atom Reorganisation	16

Abstract

Quantum dots are an example of a nanomaterial which are used for their size-tunable optoelectronic properties. There is an active body of computational and experimental research surrounding indium phosphide quantum dots (InP QDs), which have been suggested as a non-toxic alternative to cadmium selenide (CdSe) QDs. Experimental methods used to investigate these properties are commonly accompanied by computational methods, frequently including the use of the Density Functional Theory (DFT) method. This KURF report was produced as part of an undergraduate summer research project and involved the use of the CP2K software package and Tier 2 HPC, Young¹. This was to approximate the configurations of 125 InP QD clusters which resided in their most stable states (geometry optimisation) using DFT. This involved an in-depth skills training in the Linux environment via tutorials and online courses and was used to submit and monitor provided InP QD clusters to a High-Performance computational facility. One observation which confirmed the real-world challenges with research of this nature was the larger computation times associated with performing geometry optimisation, due to the larger number of electrons present within these systems. Since the relaxation time of these structures was larger than anticipated, five structures for which calculations had been completed were selected, between the ranges of 8 and 132 atoms in size. The minimum Root Mean Square Deviations (RMSDs) of these structures were calculated using Python, to quantify the extent to which they were similar to their initial versions prior to geometry optimisation. The structural changes within these QDs were also compared by producing visual representations of them with VMD. While a visual compression-like effect was observed in all five structures, their minimum RMSDs varied widely and regardless of the number of atoms. Finally, the 125 structures which geometry optimisation was performed on observed a success rate of 36.8%, indicating the need for further repeats of these calculations in future research. This project highlights the importance and associated challenges with research of this nature, with further research aiming to form a database of these relaxed structures to train a machine learning model and the theory of ab-initio molecular dynamics (AIMD) explored as an extension to the report.

¹We are grateful to the UK Materials and Molecular Modelling Hub for computational resources, which is partially funded by EPSRC (EP/P020194/1 and EP/T022213/1)

1 Introduction

1.1 An Introduction to Indium Phosphide Quantum Dots

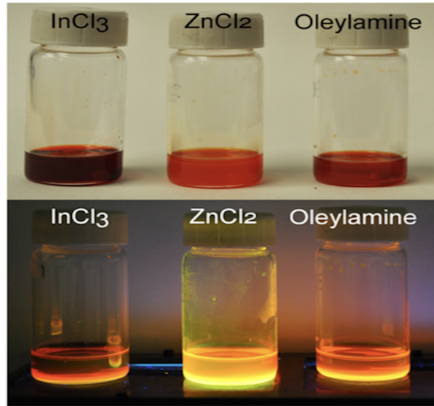


Figure 1: Experimental images showing fluorescence of colloidal InP QDs, coated with different ligands (figure reproduced from Source [1])

Materials development is a significant and growing area of research, which involves the study of structure-property relationships to enable the new applications. An important role in this research is played by nanomaterials, which are defined as systems whose particles are up to 100 nm in size [2]. Among nanomaterials, quantum dots (QDs) are of particular interest because their properties may be controlled by altering their geometries and chemical compositions. Knowledge of their inner workings allows for QDs to be engineered for a multitude of applications [3]. These may broadly be categorised as being optical (bioimaging, optical fibre systems and lasers) and electronic (LED displays, thermoelectric devices and renewable energy solutions) in kind [1,4-6]. There is currently an active body of research which uses various methods to garner information about these optoelectronic properties, to ensure that the QDs may be better used for these applications.

QDs are comprised of a semiconductor core and, in some cases, an outer shell to fine-tune their properties. These semiconductors are materials whose electrical conductivities are between those of conductors and insulators [4]. While we later explore their structures in more depth, semiconductor research is paramount to offering more competitive materials for QD applications. While these QDs have seen twenty years of research improving their efficiencies and brightness, particular attention is being paid to InP QDs as a non-toxic alternative [5]. This is due to cadmium's toxicity, regulations regarding this and the broader colour emission of InP QDs when using their structure-property relationships [6, 7]. These differences are because CdSe is more ionic, although more research is required to determine specificities [5] and is implemented in a variety of ways.

Approaches used in cutting-edge research to investigate QD properties include experimental, computational, and theoretical methods. This is where numerical techniques have been applied computationally, to verify experimental results [8] and to offer more convenient methods of investigating the dots in cases where experimental limitations exist. For instance, in the case where it is difficult to prepare homogeneous QDs experimentally, then their properties may be simulated [7], and to simulate material behaviour under high temperatures or conditions which may be difficult to experimentally obtain [6]. These numerical techniques generally fall into

two categories, classical molecular dynamics (MD) and ab-initio ('from the beginning') techniques. Among the favoured methods to research these systems is ab-initio molecular dynamics (AIMD²), which is implemented as an extension of the widespread Density Functional Theory (DFT) method. AIMD is used to simulate InP QDs in literature as it reduces the amount of fitting required during simulation processes [9]. With this said, practical implementations of MD do not exist without challenges.

These are later explored and include instances where experimental and simulated results are not within reasonable agreement. This is owing to inconsistencies in the numbers of atoms which are present in experimentally produced structures. Since the optical properties of these structures is heavily dependent on their compositions and geometries, these inconsistencies introduce difficulties when computing the optical properties of experimentally produced structures. This issue is magnified when considering nanomaterials, as variations in the number of atoms present becomes more significant when determining these properties. Another important factor which must be considered when implementing these calculations is the size of the system being studied. This is because of the dependency of computational budgets on the size of systems being simulated, limiting the use of ab-initio methods to smaller systems.

It is then established that firstly, there exists the need for InP QDs as a non-toxic alternative to CdSe. Secondly, that there is a smaller body of research regarding the computational application of MD techniques to InP QDs than their bulk counterparts [6]. This has given rise to the need for a furthered body of computational research surrounding structure-property relationships within InP QDs. Although, it is important to first explore the structure of InP in more depth, in bulk and as a nanomaterial.

1.2 The Structure & Properties of Crystalline InP

1.2.1 Structure & Bonding Within InP

A useful way to describe materials is by using their spatial distributions. Where crystalline structures can be described as systems with long-range order, amorphous materials exhibit local-range order or none [10].

In the case of InP, a zinc-blende structure has been measured. Atoms may be arranged within this cell following a face centred (FCC) distribution as shown in Figure 2 (c). This may be repeated to produce a crystalline structure similar to those shown in Figures 2 (a) and (b). This unit cell has a density ρ of 4.81 g/cm³ [11] and consists of repeating units of indium and phosphide fcc lattices, which have been shifted relative to each other.

The crystalline structure of InP is comprised of indium and phosphorus, being a trivalent metal and tetravalent non-metal respectively [13]. One s and three p orbitals combine to produce sp^3 orbital hybridisation when these elements bond, due to their electron configurations [11]. This is also referred to as tetrahedral hybridisation, as each atom contains four of these sp^3 orbitals [2]. This results in orbitals whose components are comprised of a mixture of s and p orbitals (25% s character and 75% of p orbital character). The bonds between indium and phosphorus also have a partial ionic character, due to a charge transfer which occurs between them, where indium has a smaller ionic character within the bonds.

1.2.2 Electronic Structure Properties of InP

The outermost shell of an atom which is occupied by electrons is its valence shell. When an electron in this band gains sufficient energy by way of external means, it may transition into another band (the conduction band). The difference in potential between uppermost part of

²See supplementary information for further details

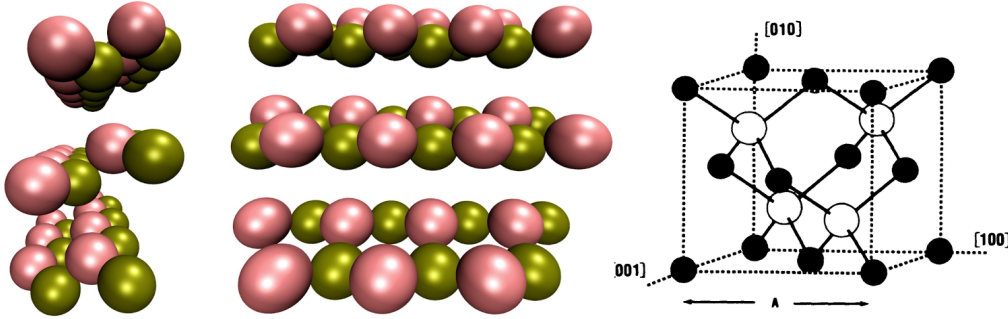


Figure 2: (a) the side-view of an InP structure consisting of 125 indium (pink) and phosphorus (green) atoms. (b) its equivalent head-on view. The zinc-blende structure of this is shown in a unit cube in (c), with black and white spheres representing indium and phosphorus atoms respectively (Figure (c) reproduced from Source [12])

the valence band and lowermost part of the conduction band is the band gap of the material determines the range of energies that electrons can have within a semiconductor [11]. These bands are also represented by the terms lowest unoccupied and highest occupied molecular orbitals (LUMO and HOMO) [6]. This is important because the band gap determines the mobility of its electrons and hence electrical conductivity. When this band gap is large, electrons are able to gain sufficient energy to transition bands. In this case, the material has limited conductive capabilities and is an insulator. In cases where the conduction and valence bands overlap, the material possesses a sea of electrons which enable it to have conductive properties. As previously mentioned, a semiconductor is a material whose electrical conductivity is between that of a conductor and insulator, implying a band gap which is also intermediary between the two [4]. This is relevant to our case because InP is referred to as a III-V type semiconductor. This is owing both to the number of valence electrons indium and phosphorus atoms have, and to the previously mentioned partial-ionic character of the bonds.

In semiconductors, if the crystal momentum is the same at the valence band maximum as the conduction band minimum, then its band gap is direct. InP is a direct band gap semiconductor and when a valence band electron migrates into the conduction band, it leaves a positive hole in the band where it initially resided to maintain charge conservation. Electrons may be influenced to transition under an external electric field, forming a current in bulk semiconductors. The impact the electric field has on the drift velocity of these charges, electrons and holes, is quantified by the mobility value of its respective material. This is where mobility refers to the magnitude of a charge's drift velocity per unit electric field [13]. This is applicable to electron-hole pairs (excitons) in direct band gap semiconductors, as they share the same electric field and their drift speeds are identical, but opposite in direction. This produces respective mobility values of $4 \times 10^3 \text{ cm}^2/\text{Vs}$ and $1.3 \times 10^5 \text{ cm}^2/\text{Vs}$ for single and polycrystalline InP structures [9].

After excitation, electrons which have migrated to the HOMO and their corresponding holes are referred to as excitons [13]. Since these are of opposite charge, they are attracted by the Coulomb force. After the lifetime of the exciton, the electron and its hole re-combine. For this to occur, the electron must de-transition back to the valence band. This recombination process is different in direct and indirect band gap semiconductors, and is critical to the excitonic properties of bulk InP.

The band gap structures of InP are shown in Figure 3 and are a result of combining indium

and phosphorus atoms to form a lattice. In comparison to other semiconductors of its type, the valence band structure of InP is similar whereas its conduction band minima differ. It is typical of other III-V type semiconductors to have conduction band minima which resemble two camel humps (a camel-back-like potential), although this is not the case with the conduction band minima of InP [11]. The conduction band minima of InP exist as higher minima (L and X) and at Γ , where the most band structure symmetry occurs and valence band minima may also exist. Electrons in the Γ_{6C} minima contribute to the conductivity of the alloy past 800K [11]. Recombination would occur in this band gap structure via direct photon emission, as the k vector (crystal momentum) of the LOMO and HOMO align [11]. This is seen in Figure 3 as the Γ_6 and Γ_8 minima and maxima have the same k value (Γ). This means that electrons may directly transition bands without having to transfer momentum into the lattice, in order for it to be conserved. In indirect band gap semiconductors, the k vector of the HOMO and LUMO do not align, meaning that electrons must change momentum in order to transition bands, and this direct photon emission is hampered. As recombination in InP occurs, the electrons in each experience a change in energy similar to its band gap. Due to this change in potential of the electron, a photon is emitted whose energy is similar to the band gap. In this case the band gap closely determines the wavelength of emitted photons, the exciton wavelength, and hence the excitonic properties of InP. Crucially, in comparison to their bulk counterparts, the smaller the size of a QD the higher the frequency of its emitted photons. This is due to quantum mechanical effects we next discuss [14].

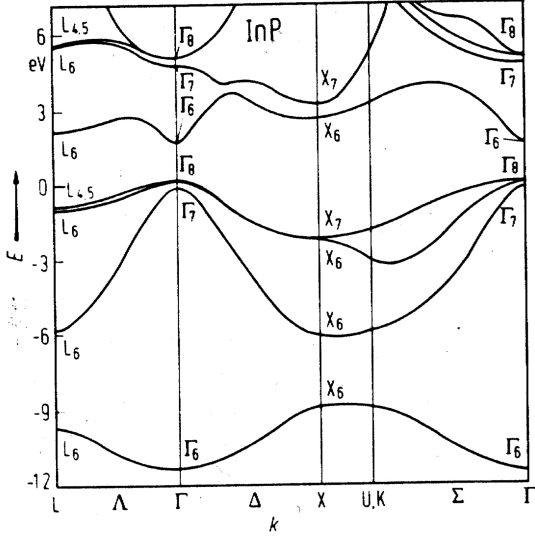


Figure 3: Graph demonstrating band-gap structure of InP (figure reproduced from Source [11]

1.3 InP QDs

1.3.1 The Structure of InP QDs

As previously alluded to, one elegant example where a material's dimensions impact its properties is that of a nanomaterial in comparison to its bulk equivalent. Although we have mentioned the crystalline structure and bonding of InP, the optoelectronic properties of its QDs are due to

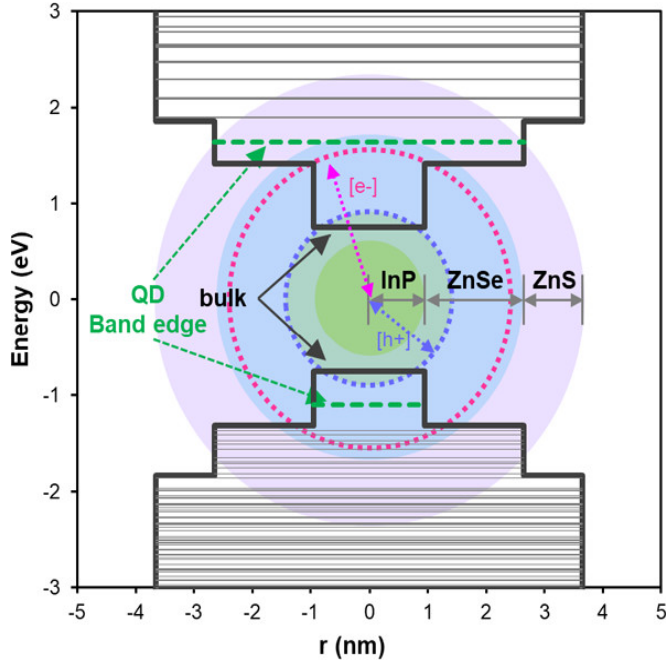


Figure 4: A graph showing how the energy of a spherical QD with an InP core and ZnSe and ZnS coatings varies with its radius. The widths of these coatings have been engineered to combine with the InP core and alter the QD band gap to produce green fluorescence (Figure reproduced from Source [15]

quantum mechanical effects. The size-dependent photon emission of QDs may be crudely understood by modelling an electron which migrates between the conduction and valence bands of the QD as being confined within an infinite square (or cubic) potential well. In this model, the energy states of the particle in the well are quantized and inversely proportional to the square of the well width. It is also important to note that for the InP QDs we investigate in this project, the relation between their exciton wavelengths and QD size is approximately inversely proportional to the QD diameters when modelled as spheres [7, 8]. This means that the smaller the well width, the higher the band gap between the conduction and valence bands. Hence, the higher the energy of the photons fluoresced for smaller well widths (produced by smaller QDs). This effect is termed the quantum confinement effect, or QCE. This may be engineered to produce QDs of different exciton wavelengths (bandgap engineering), with QDs around 2 nm in size emitting violet light and 10 nm in size emitting red light [14]. These size-tunable features of QDs allow for their promising optical applications, such as narrow bandwidths of emitted photons, controllable emission spectra, and their broad spectral ranges [8].

Further, InP QDs in literature exist in a range of sizes and chemical compositions. It is expected that the size of QDs are of the order of nanometres, since they are nanoparticles. In one paper by Micic et al, the size-dependent spectroscopy of spherical InP QDs were investigated, in which their diameters varied between between 2.6 nm and 6 nm [16]. The size of QDs relaxed by this project exist as clusters of InP between 111 and 555 atoms, each forming a QD. These cluster sizes are selected to resemble the QDs used in experiments.

Computationally generated InP QDs may also be made to exist in various shapes such as cubes, cuboctahedra and tetrahedra, although only spherical InP QDs have been experimentally

1.3 InP QDs

confirmed as possible. The possible shapes of computationally generated InP QDs are also limited due to their charge neutrality [5]. As previously mentioned, QDs may be surrounded by amorphous shells for use within certain contexts (for use in biological imaging and to prevent toxicity of the dots for instance). The orange fluorescence of one type of colloidal InP QD lies within the 480 nm region [1] and is also shown by Figure 1. Although, this may vary according to various factors including the dot coating, the core uniformity, the electron-hole distribution within the QD and if it has been doped with other atoms [15]. These important factors are controlled when manipulating the structure-property relationships of these systems. The chemical composition of a common InP QD type found in literature is that of an InP core, surrounded by a ZnSe and or ZnS coating (Figure 4). In one example, Jang et al experimentally varied the width of these layers to produce different exciton wavelengths [15]. This was when the InP core of these QDs was varied between 1 nm and 1.75 nm, the ZnSe shell between 1.7 nm and 1.8 nm and its ZnS outer shell between 0.2 and 1 nm. The amorphous shells of some experimentally produced InP QDs also produce trap states, which have been investigated with techniques we explore in the next section.

Further, there are numerous methods of generating these clusters computationally. One method used computationally by Zaho et al was using high-temperature AIMD³. The clusters this within this report were first generated computationally using a different method, which Figure 5 shows.

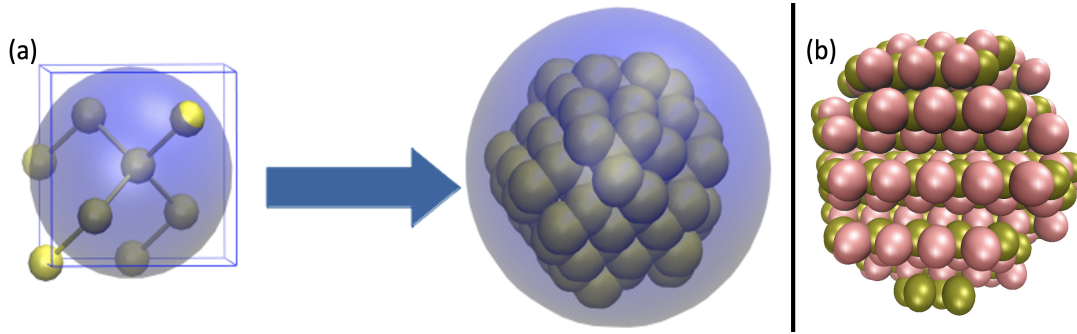


Figure 5: A diagram showing the creation of InP QDs this report uses. This is by first creating various repetitions of particles in a cube within Cartesian space (Figure 5 (a) LHS).

Atoms on the extremities of a sphere fit within this cube are next removed (Figure 5 (a) RHS), producing a cluster of crystalline InP molecules representing a QD. In this example, a QD of 555 atoms has been produced and is the largest relaxed in this report (Figure 5 (b))

1.3.2 Numerical Techniques For Simulating InP QDs

DFT has been widely used to research the mechanical and optical properties of InP QDs. This was exemplified by Cho et al, who used it to determine a relation between the dot size and its QCE [7]. The theory used to achieve this included EMAs (Effective Mass Approximations) and the Particle In a Box (PIB) model we have mentioned [7]. Interestingly, a particle-in-a-sphere model was used by Snee et al for conduction states [1]. This method uses a radial potential, as opposed to a simple particle in a box analogy to understand the QDs. Further, Cho et al relied on several assumptions including modelling the interface potential between QDs and

³See supplementary information for further details

their ligands as hard walls [7]. Another endeavour was achieved by Dumbgen et al, who used the technique to investigate trap states of the QDs due to undercoordinated surface atoms in InP clusters. This was important since their Photoluminescence Quantum Yields (PLQY) were dependant on emissions associated with these atomic trap states [5].

A third instance where DFT has been applied was by Ma et al to determine the optoelectronic properties of InP QDs [8]. This included their exciton binding energies, decay lifetimes and optical absorption spectra. It is noted that Ma et al used time-dependent DFT (TDDFT) in addition to DFT to establish these properties [8]. A final use of DFT in literature which we mention was its application by Snee et al to characterise surface defects in colloidal InP QDs after experimental data had been gathered [1]. Significantly, computational results obtained using the technique, in this case, did not align with their experimental counterparts. Such challenges associated with these numerical techniques are explored at the end of this section.

The second numerical technique used to investigate InP QDs we mention is AIMD, as applied by Zhao et al [6]. This research used high-temperature MD to relax InP nanostructures into amorphous clusters. The energy of bulk InP geometries optimised using spherical models is typically higher than these QDs. This was important in this case because InP QDs are surrounded by amorphous shells which may limit their growth [6].

1.3.3 Challenges When Simulating InP QDs

We first return to the previously mentioned case of Snee et al [1], curiously whose simulation results when using DFT to characterise surface defects in colloidal InP QDs did not align with their experimental counterparts. This was attributed to a shortage of sufficient surface passivation of QDs within their models and was consistent across various studies. This includes those of Gary et al [1] and indicates the need for further research within the field.

The most predominant challenge when using DFT to simulate InP QDs is that the computational time required to perform it is of a quadratic order with respect to the number of electrons in the system [9]. The simulation of larger structures is therefore computationally expensive using this technique. This means that it is difficult to use it to simulate QDs which are the size seen experimentally, specifically in realistic environments. There is also a need for further research to determine a classical forcefield which may accurately model this phenomena in classical simulations.

Finally, one challenge mentioned by Zhao et al when using high-temperature MD to model InP QDs is the modelling of amorphous shells which surround their crystalline cores and limit their growth [6]. There exists a limited body of research specifically surrounding amorphous InP nanomaterials at low energies. Further, computational methods commonly used to obtain this information for other nanomaterials have challenges of their own. One method to address this is the coalescence kick method, which first randomly situates atoms at a distance. This distance is reduced at speed as atoms move towards their common centre of mass, form a cluster and undergo optimisation via DFT. This process is repeated and the most stable configuration selected. This however requires excessive computational resources, limiting its use to smaller systems. Other solutions include minimum hopping methods to avoid the recurrence of minima via this method, and Monte Carlo methods.

As established, in this section we have discussed the need for deliberate efforts to apply computational methods to simulate the properties of nanomaterials, since these are often different from their bulk counterparts. One example introduced was InP, with discussed electronic structure properties among others. While numerical techniques to simulate InP QD properties exist, literature for two methods (AIMD and DFT) was reviewed.

2 Results & Analysis

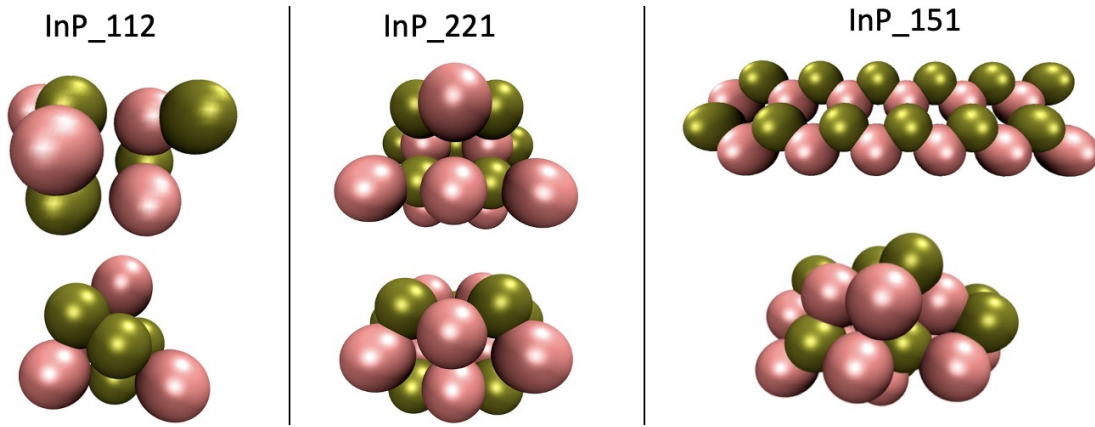


Figure 6: Diagram showing three InP clusters (InP_112, InP_221 and InP_151), each with less than 100 atoms. Top: prior to geometry optimisation. Bottom: following geometry optimisation

Structure	Minimum RMSD/ \AA	Number of Atoms (n)
InP_112	1.54	8
InP_221	0.99	16
InP_151	1.45	24
InP_432	1.58	100
InP_253	0.30	132

Table 1: table showing Root Mean Square Deviation of five relaxed InP clusters and the number of atoms in each structure

Five InP clusters varying between 8 and 132 atoms in size (see Table 1) have undergone geometry optimisation in this report, to ensure that they are configured in a more energetically favourable way. Skills training provided as part of the KURF for this to be implemented included Linux and Bash training through tutorials and online courses. 125 previously generated InP QD clusters were provided, which were produced with the method Figure 5 shows. These were submitted to the Tier 2 supercomputer, Young⁴. This was done so by submitting the clusters in groups of 25, for relaxation with the CP2K software package and required the implementation of provided training. The progress of these optimisations was monitored daily and the final data downloaded from the supercomputer following the completion of all calculations. It is notable that one of the challenges mentioned while performing geometry optimisation on these structures is the larger computational times associated with bigger systems, particularly as the number of electrons within these systems increase. These structures took longer than anticipated to undergo geometry optimisation, and therefore five optimised structures were selected before all had been fully relaxed, so that their RMSDs could be compared to draw

⁴We are grateful to the UK Materials and Molecular Modelling Hub for computational resources, which is partially funded by EPSRC (EP/P020194/1 and EP/T022213/1)

conclusions from in this report. This highlights the larger computational times associated with the use of DFT to perform geometry optimisation as system sizes increase. This was also corroborated by a success rate of 36.8% of all structures geometry optimisation was performed on, with 46 of the 125 inputted structures successfully optimised. This indicates that these calculations are required to be re-computed until this success rate reaches 100%.

When plotted in VMD, a visual representation of a cluster may be made prior to and following atom reorganisation, to compare their differences. This difference varied widely across all relaxed clusters (see Figure 8). This comparison also loosely appears more visually pronounced in the three clusters with less than 100 atoms (Figure 6), with respect to clusters with more than 100 atoms (Figure 7). This difference also appears larger in structures which had less spherical symmetry when unrelaxed (InP_151) and may be quantified using the minimum Root Mean Square Deviation (RMSD) method.

The Cartesian coordinates of the i^{th} atom in an n atom cluster following geometry optimisation are (x_i, y_i, z_i) . The position of the unrelaxed (reference) state of this atom is $(x_{i,ref}, y_{i,ref}, z_{i,ref})$. In this case, the residuals of the atom are the difference between its Cartesian coordinates prior to and after geometry optimisation. The distance which the atom has moved following geometry optimisation is given by Pythagoras's theorem using these coordinates. For equally weighted atoms in a cluster, the distance the average atom has moved following atom reorganisation is the RMSD of the cluster (given by Equation 1). A large RMSD therefore implies a lower level of similarity between the initial and relaxed geometries. This is due to differences which form during relaxation such as the relative rotation of the position of atoms in the cluster or translation of atoms due to bonds which form during the relaxation process.

The minimum RMSD is an important measure of the similarity of a structure to its reference state. While the RMSD is a measure of how much the atomic coordinates of the average atom in a cluster differs following optimisation, this may be arbitrarily high due to translational and rotational differences between the coordinates of the structures caused by relaxation, which are inconsistent across different relaxed clusters. The Kabsch algorithm is implemented using Python to minimise the RMSD of each cluster, to quantify the movement of its mean weighted atom after atom reorganisation while accounting for these effects. This ensures that the minimum RMSD is a viable means of comparison across clusters and is shown in Table 1.

$$RMSD = \sqrt{\frac{\sum_n[(x_i - x_{i,ref})^2 + (y_i - y_{i,ref})^2 + (z_i - z_{i,ref})^2]}{n}} \quad (1)$$

The computational method used to minimise the RMSD for a cluster is comprised of three stages. Following relaxation, there are two sets of atomic coordinates for each cluster (one each for before and after optimisation). When each set is placed into a matrix, each cluster has two $3 \times N$ matrices. The premise of this method is to perform transformations on these matrices, and hence transform the coordinates of the atoms to coincide in the position of minimum RMSD for the cluster. Firstly, the two structures are re-centred so that their weighted mean coordinates (centroids) align, which are used as the origin of their coordinate systems. This corresponds to a translation on these matrices and removes unnecessary distance between structures which may increase the RMSD of the cluster. The second and third stages of this use matrix equations to calculate the optimal rotation matrix, to map the configurations onto each other. This process is referred to as singular value decomposition and is computed using Python. This results in two matrices with the atomic coordinates of the cluster, prior to and following geometry optimisation, which produce the minimum RMSD when operated on.

Although we previously explored the visual dichotomy between unrelaxed and relaxed clusters in Figures 6 and 7, this allows for this difference to be quantified in Table 1. This confirms

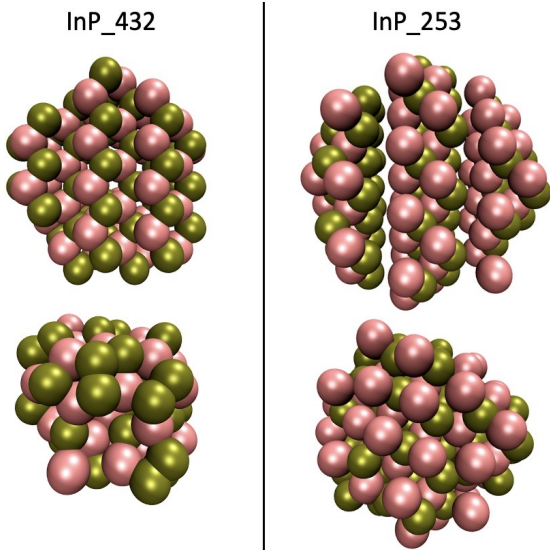


Figure 7: Graph demonstrating band-gap structure of InP (figure reproduced from Source [11]

the visual implication that the change in the relaxed and unrelaxed geometries varied widely. In fact, the cluster with the largest minimum RMSD was InP_112, with the smallest number of atoms, and cluster with the second largest minimum RMSD had the second largest number of atoms. While both clusters with more than 100 atoms showed variability in their minimum RMSDs (the minimum RMSD of InP_432 was over five times that of InP_253), their visual representations both demonstrated the crystalline structure seen in their unrelaxed states undergo a compression-like effect into more stable states. This demonstrates the need to quantify the minimum RMSD of these structures, in order to better compare them. This compression-like effect was also seen visually, and particularly in InP_151 with little spherical symmetry. All minimum RMSDs were also of similar orders of magnitudes, implicating a lack of outliers. The largest minimum RMSD concerned InP_112, indicating that its initial unrelaxed state was the least stable in comparison to its state following geometry optimisation.

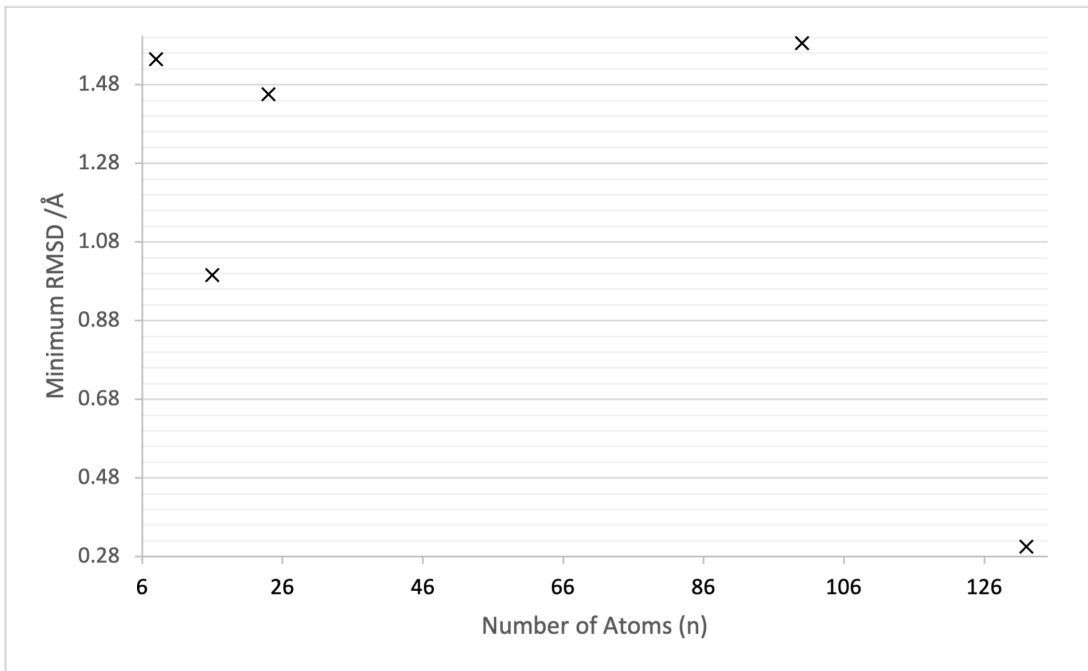


Figure 8: A graph demonstrating the large variation of the minimum RMSD with the number of atoms per InP cluster geometry optimisation was performed on

3 Conclusion

This report first introduced the importance of QD research for obtaining information regarding their size-tunable optoelectronic properties, and InP QDs as a non-toxic alternative to CdSe QDs. The structure and bonding of InP was next discussed, with InP being explored as a direct bandgap semiconductor. This was extended to quantum mechanical effects introduced for InP QDs, allowing for these properties. The computational method used to generate QDs used in this report was next mentioned and DFT was introduced as a method of performing geometry optimisation on these clusters.

The importance and challenges associated with DFT were next explored in literature, with particular importance being placed on the computational time required to optimise larger structures. This challenge was of importance because the 125 InP clusters optimised as part of this project using the Tier 2 HPC, Young and CP2K software package took longer than anticipated to perform these calculations. This was owing to the success rate observed in our sample, which indicates that many rounds of calculations are needed to obtain a success rate of 100%. This exemplifies the challenges associated with performing real-world research of this nature and with MD methods. Five optimised structures varying between 8 and 132 atoms were thus selected and visualised using VMD and their minimum RMSDs calculated using Python, to quantify this difference. Skills training used when doing so included VMD, Linux and Bash via provided tutorials and online courses.

It was found that the largest minimum RMSD was associated with InP_112, with the smallest number of atoms - indicating that its initial unrelaxed state was the least stable in com-

parison to its state following geometry optimisation. Meanwhile, the smallest minimum RMSD belonged to InP_253 - with the most amount of atoms, indicating the opposite was true in this case. Despite this, there was interestingly a wide variability between all minimum RMSDs observed, as structures formed new bonds in their more stable states. This was a finding which was consistent across the structures when visualised using VMD, although all structures observed a compression-like effect when optimised, into seemingly random - but more stable states. This effect visually appeared most similar in the two clusters with more than 100 atoms each (InP_432 and InP_253) despite their considerably different minimum RMSDs. This effect was also visually pronounced in InP_151, whose unrelaxed equivalent had little spherical symmetry.

This project highlights the importance of research of this nature, with further research aiming to form a database of these relaxed structures from which to train a machine learning model and perform further calculations. This also highlights the challenges faced when performing DFT to perform geometry optimisation on InP QDs, and shows the observable compression-like effect which they undergo when this is performed across structures between 8 and 132 atoms in size. A further extension of this work is via the application of AIMD, whose theory is explored in the supplementary information within this report.

References

- [1] Preston T. Snee. Dft calculations of inp quantum dots: Model chemistries, surface passivation, and open-shell singlet ground states. *The Journal of Physical Chemistry C*, 125(21):11765–11772, 2021.
- [2] Mark T. Weller and Tina Overton. *Inorganic Chemistry*. Oxford University Press, 7 edition, 2018.
- [3] Andrew M. Smith and Shuming Nie. Semiconductor nanocrystals: Structure, properties, and band gap engineering. *Accounts of Chemical Research*, 43(2):190–200, 2009.
- [4] Robert Curley. Semiconductor. *Britannica*, Aug 2022.
- [5] Kim Corinna Dümbgen, Juliette Zito, Ivan Infante, and Zeger Hens. Shape, electronic structure, and trap states in indium phosphide quantum dots. *Chemistry of Materials*, 33(17):6885–6896, 2021.
- [6] Qing Zhao, Lisi Xie, and Heather J. Kulik. Discovering amorphous indium phosphide nanostructures with high-temperature ab initio molecular dynamics. *The Journal of Physical Chemistry C*, 119(40):23238–23249, 2015.
- [7] Eunseog Cho, Hyosook Jang, Junho Lee, and Eunjoo Jang. Modeling on the size dependent properties of inp quantum dots: A hybrid functional study. *Nanotechnology*, 24(21):215201, 2013.
- [8] Xiaoyu Ma, Jingjing Min, Zaiping Zeng, Christos S. Garoufalidis, Sotirios Baskoutas, Yu Jia, and Zuliang Du. Excitons in inp, gap, and $ga_xin_{1-x}P$ quantum dots: Insights from time-dependent density functional theory. *Phys. Rev. B*, 100:245404, Dec 2019.
- [9] Michael P. Allen. *Introduction to Molecular Dynamics Simulation*, volume 1. Centre for Scientific Computing and Department of Physics, University of Warwick.
- [10] Averill et al. *12.1: Crystalline and Amorphous Solids*. Chemistry LibreTexts.
- [11] Heesuk Rho. *Indium Phosphide (InP)*, volume 1. University of Cincinnati, 45221 edition, 1995.
- [12] Carlos Barrios. Gallium arsenide based buried heterostructure laser diodes with aluminium-free semi-insulating materials regrowth doctoral thesis by. 09 2022.
- [13] Charles Kittel. *Introduction to solid state physics*. Wiley, 1996.
- [14] Wolfgang J. Parak. *Fundamental Principles of Quantum Dots*. Wiley Online Library, 2010.
- [15] Eunjoo Jang, Yongwook Kim, Yu-Ho Won, Hyosook Jang, and Seon-Myeong Choi. Environmentally friendly inp-based quantum dots for efficient wide color gamut displays. *ACS Energy Letters*, 5(4):1316–1327, 2020.
- [16] O. I. Mićić, H. M. Cheong, H. Fu, A. Zunger, J. R. Sprague, A. Mascarenhas, and A. J. Nozik. Size-dependent spectroscopy of inp quantum dots. *The Journal of Physical Chemistry B*, 101(25):4904–4912, 1997.

4 Supplementary Information

4.0.1 Theory for Atom Reorganisation

As an extension to this report, this supplementary section explores the theory of MD and the use of AIMD by Zhao et al to simulate InP clusters in more depth.

For a given system of atoms, MD uses an iterative process to classically solve its equations of motion (Equation 2). This is where the mass, forces on and displacement of the i^{th} atom in the system are represented by m , \mathbf{f}_i and \mathbf{x}_i respectively [9]. To compute the values of \mathbf{f}_i , it is necessary to first determine the potential \mathcal{V} of the system. This is a function of the Cartesian coordinates of atoms in the system, when their rotational degrees of freedom are neglected. Interactions between atoms may be thought of as being bonded or non-bonded in nature. \mathcal{V} is therefore considered in terms of these bonded and non-bonded potentials. The latter is obtained through a summation [9], which considers i^{th} body interactions within the system. This may include the Coulomb potential, Lennard Jones potential or the impact of container walls on \mathcal{V} , depending on the system.

$$m_i \ddot{\mathbf{x}}_i = \mathbf{f}_i \quad \mathbf{f}_i = -\frac{\partial}{\partial \mathbf{x}_i} \mathcal{V} \quad (2)$$

Bonding potentials contribute to \mathcal{V} specifically in cases where the system contains molecules. In this case, the Coulomb potential and molecular bonds are better modelled by the introduction of electrostatic multipoles. Among others, three things are considered when calculating this bonded contribution to \mathcal{V} . Firstly, the total contribution of the bonds themselves, which may be harmonic. Secondly, how angles between different bonds (multipoles) combine to add to this potential, which depends on the distances of atoms to their equilibria positions and may be of quadratic form. Thirdly, torsion angles [9] between bonded multipole pairs, which are the angles between planes in which they reside. These are obtained via software packages which use vector calculus equations. These packages also consider other parameters, which Allen mentions may rely on quantum chemical calculations and additional force fields with their own use cases and accuracies. This information regarding the non-bonded and bonded potentials of our system is combined to obtain \mathcal{V} . This is used in conjunction with Equation 2, resulting in several PDEs which may be solved by hand for simple systems and computationally for more complex ones. From this, values of \mathbf{f}_i are determined, in turn from which the force field of the system may be modelled.

A second method to solve the equations of motion for these systems is using an approach with a Hamiltonian (\mathcal{H}). This uses an iterative numerical method to solve Equation 3, where \mathbf{p}_i refers to the momentum of the i^{th} particle in the system. These equations may be solved iteratively via the Verlet algorithm. This converts them into linear forms, to computationally solve for \mathbf{p}_i and \mathbf{x}_i , and later for \mathbf{f}_i . This is computationally demanding because calculating values of \mathbf{f}_i may rely on sums of pairs of atoms [9]. One reason this algorithm is preferred is that the equations it uses for iterations are linear. This allows for the use of larger timesteps and so for it to better adapt to this challenge.

$$\begin{aligned} \dot{\mathbf{x}}_i &= \mathbf{p}_i/m_i \\ \dot{\mathbf{p}}_i &= \mathbf{f}_i \\ \mathcal{H} &= \mathcal{V} + \frac{1}{2m_i} \sum_{i=1}^N |\mathbf{p}_i|^2 \end{aligned} \quad (3)$$

Various constraints are introduced while doing so because these are classical approximations of quantum systems. While in a quantum mechanical model bonds would have high vibrational

frequencies, in this approximation their bond lengths are fixed (as opposed to being modelled via springs). This is achieved by introducing systems of constraint equations which may be solved iteratively [9] and gives rise to fewer complexities mathematically than by using a spring model for the bonds. One important development Allan mentions when introducing these constraints within the Verlet algorithm is by ensuring that they are fulfilled precisely at the end of each iteration of the algorithm, referred to as ‘SHAKE.’ Before this development, this would have instead seen the use of the method ‘RATTLE.’

A second constraint used is boundary conditions. These are likely to be periodic if the system is comprised of fewer atoms, as more of them face the outside of the system in this case. Allan further mentions the concept of a simulation box, which effectively surrounds the system with multiples of itself to do so. This is of use if atoms are situated closer to the box extremities. For larger systems, this may be adapted into a cubic simulation box divided into cells. Additional methods may be used to extend this, such as involving the introduction of time dependence via the Louiville operator. It is important to use timesetps here which are small enough to model rapidly occurring phenomena, depending on the context. Allan also mentions that Verlet’s algorithm conserves volume in phase space (it is symplectic), which produces convenient results within the algorithm’s mathematics, and is time reversible. In practice, this MD may be conducted under various conditions.

As previously mentioned, an example where this technique was used in practice was by Zhao et al, to relax InP nanostructures into amorphous clusters [6]. In this case, their formation was achieved using high-temperature MD. This initially saw the distances between atoms increasing, plateauing and decreasing due to the formation and buckling of isolated planar InP sheets into stabilised clusters. This resulted in structures, which were of lower energies and hence more energetically and mechanically favourable when opposed to their initial states [6].